J|A|C|S
ARTICLES
Published on Web 02/08/2003

Aspects of Enantioselective Heterogeneous Catalysis: Structure and Reactivity of (*S*)-(−)-1-(1-Naphthyl)ethylamine on Pt{111}

Jonathan M. Bonello,† Federico J. Williams, and Richard M. Lambert*

Contribution from the Department of Chemistry, University of Cambridge, Cambridge CB2 1EW, U.K.

Received September 6, 2002; E-mail: rml1@cam.ac.uk

Abstract: The molecular orientation, spatial distribution, and thermal behavior of the powerful chiral catalyst modifier precursor (*S*)-naphthylethylamine adsorbed on Pt{111} have been studied by NEXAFS, XPS, STM, and temperature programmed reaction. At 300 K, both in the presence and in the absence of coadsorbed hydrogen, the strongly tilted molecules do not form ordered arrays. These results constitute the first direct evidence against the template model and are at least consistent with the 1:1 interaction model of chiral induction in the enantioselective hydrogenation of alkyl pyruvates. Raising the temperature beyond 320 K (the temperature of enantioselectivity collapse) leads either to irreversible dimerization with hydrogen elimination or to dissociation of the ethylamine moiety, depending on whether coadsorbed H_a is present. Either way, the stereogenic center is destroyed. These findings provide the first direct clue as to the possible origin of enantioselectivity collapse, by a mechanism not previously considered. When NEA and methyl pyruvate are coadsorbed in the presence of H_a, STM reveals entities that could correspond to a 1:1 docking complex between the prochiral reactant and the chiral modifier.

1. Introduction

Heterogeneously catalyzed enantioselective reactions are of great interest because of the academic challenge they pose and because their potential technical importance is huge.[1−4] Although their number is increasing steadily, few examples of such processes are well established, and the subject as a whole remains at a relatively early stage of development.[5−8] This is especially true in regard to fundamental studies of the surface phenomena involved.

Enantioselective α-ketoester hydrogenation over platinum catalysts modified by treatment with cinchona alkaloids was first reported in 1979 by Orito et al.[9,10] Since its discovery, the reaction has been intensively studied (see, for example, refs 5 and 11−13 and references therein), and important advances in understanding have emerged. Much of this work has been carried out using cinchonidine or similar materials as the chiral modifying agents, although more recently the use of simpler and equally powerful synthetic modifiers, for example, naphthylethylamine (NEA), has emerged,[14,15] as illustrated in Scheme 1.

Here, a chiral species (for example, the *S* enantiomer of NEA) somehow acts to endow the otherwise achiral metal surface with the ability to enantioselectively hydrogenate the prochiral reactant (methyl pyruvate) to (*S*)-methyl lactate with high enantiomeric excess; correspondingly, use of (*R*)-NEA produces the (*R*)-lactate. Key questions remain to be answered before a reliable reaction model for the asymmetric hydrogenation of alkyl pyruvates on chirally modified Pt surfaces can be developed further, particularly with regard to the phenomena that underlie chiral induction. It is here that direct spectroscopic and microscopic observations on relevant adsorbed species can play a part. Indeed, we have already shown[16] that such direct measurements on the adsorbed reactant (methyl pyruvate) provide direct and clear evidence of the origin of catalyst poisoning and poor start-up.

† Present address: Firmenich SA, Rue de la Bergère 7, CH-1217 Meyrin 2, Geneva, Switzerland.

(1) Collins, A. N.; Sheldrake, G. N.; Crosby, J. *Chirality in Industry: The Commercial Manufacture and Applications of Optically Active Compounds*; John Wiley: New York, 1995.
(2) Noyori, R. *CHEMTECH* **1992**, *22*, 366.
(3) Jannes, G.; Dubois, V. *Chiral Reactions in Heterogeneous Catalysis*; Plenum Press: New York, 1995.
(4) Blaser, H. U.; Baiker, A. In *Handbook of Heterogeneous Catalysis*; Ertl, G., Knötzinger, H., Weitkamp, J., Eds.; VCH Publishers: Weinheim, 1997; Vol. 5, p 2422.
(5) Simons, K. E.; Meheux, P. A.; Griffiths, S. P.; Sutherland, I. M.; Johnston, P.; Wells, P. B.; Carley, A. F.; Rajumon, M. K.; Roberts, M. W.; Ibbotson, A. *Recl. Trav. Chim. Pays-Bas* **1994**, *113*, 465.
(6) Blaser, H. U.; Jalett, H.-P.; Müller, M.; Studer, M. *Catal. Today* **1997**, *37*, 441.
(7) Baiker, A. *J. Mol. Catal. A: Chem.* **1997**, *115*, 473.
(8) Wells, P. B.; Wilkinson, A. G. *Top. Catal.* **1998**, *5*, 39.
(9) Orito, Y.; Imai, S.; Niwa, S.; Hung, N. G. *J. Synth. Org. Chem. Jpn.* **1979**, *37*, 173.
(10) Niwa, S.; Imai, S.; Orito, Y. *J. Chem. Soc. Jpn.* **1982**, 137.
(11) Wehrli, J. T.; Baiker, A.; Monti, D. M.; Blaser, H. U. *J. Mol. Catal.* **1989**, *49*, 195.
(12) Augustine, R. L.; Tanielyan, S. K.; Doyle, L. K. *Tetrahedron: Asymmetry* **1993**, *4*, 1803.
(13) Margitfalvi, J. L.; Tfirst, E. *J. Mol. Catal. A: Chem.* **1999**, *139*, 81.
(14) Heinz, T.; Wang, G.; Pfaltz, A.; Minder, A.; Schürch, M.; Mallat, T.; Baiker, A. *J. Chem. Soc., Chem. Commun.* **1995**, 1421.
(15) Minder, A.; Schürch, M.; Mallat, T.; Baiker, A.; Heinz, T.; Pfaltz, A. *J. Catal.* **1996**, *160*, 261.
(16) Bonello, J. M.; Lambert, R. M.; Künzle, M.; Baiker, A. *J. Am. Chem. Soc.* **2000**, *122*, 9864.

10.1021/ja028436x CCC: $25.00

Scheme 1

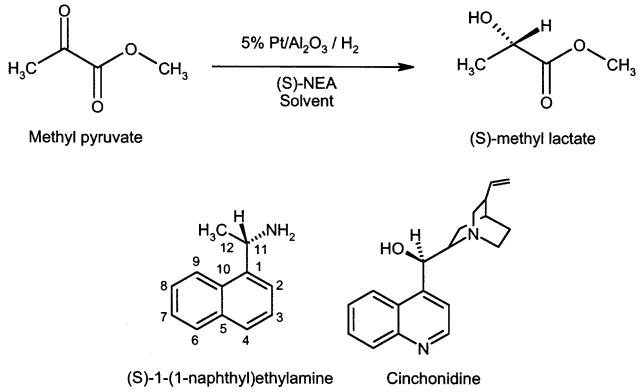

All known effective chiral modifiers for the Orito reaction contain a quinoid or naphthyl function attached to a chiral group, and it is widely believed that these aromatic "footprints" serve to anchor the chiral moiety to the catalytic surface in an appropriate manner, yet to be determined. Accordingly, we have previously investigated the adsorption geometry, spatial distribution, and chemical reactivity of quinoline and lepidine (4-methylquinoline) on Pt{111}.[17,18] These species were chosen to examine the effect on adsorption geometry of increasing the size of the substituent at equivalent positions of the naphthyl and quinoid ring systems (1- and 4-, respectively, see Scheme 1), an issue that is also relevant here.

In the present paper, we report the corresponding behavior of NEA itself. We bear in mind that under catalytic conditions NEA reacts with pyruvate to produce a secondary amine, which then acts as the actual chiral modifier. This material cannot be handled in a vacuum, so to this extent one may say our measurements are one step removed from reality. However, viewed as an extension of our previous work, they are one step closer to reality. Additionally, we may note that recent studies in a solution of NEA[19] and NEA + pyruvate[20] on Pt{111}-{211}{331}{643} single-crystal surfaces reveal that the adsorption behavior of NEA and the secondary amine derived from it are essentially the same.

Here we address the following issues. First, what is the molecular orientation of NEA on Pt{111}, and how is it distributed spatially? Such information should help us to understand how chiral induction arises in the enantioselective reaction. Second, what is the cause of the irreversible transition from enantioselective to racemic hydrogenation that occurs above ~320 K? Accordingly, we have studied the behavior of (*S*)-NEA on a well-characterized Pt{111} surface, in the absence and in the presence of coadsorbed hydrogen, by means of NEXAFS, XPS, STM, and temperature programmed reaction (TPR). The {111} surface was chosen because in practice it is found that the enantioselective reaction proceeds efficiently only on Pt particles whose size exceeds 3 nm,[21] suggesting that the low index planes of the metal dominate its behavior in chiral catalysis.

2. Experimental Procedure

Full experimental details have been published elsewhere[17,18] concerning the laboratory-based and synchrotron measurements. The XP and NEXAFS spectra were obtained on beamline 1.1 at the Daresbury SRS, and surface concentrations of adsorbed species and stoichiometric ratios were determined from the integrated intensities of the adsorbate and substrate core levels using standard analysis methods.[22] NEXAFS spectra at the carbon K-edge were acquired in partial electron yield mode at a photon energy resolution of ~0.5 eV. Repeated experimental measurements showed that the error in the estimated molecular tilt angle, α, was on the order of $\pm 5°$. The system base pressure during capillary dosing of (*S*)-NEA and during spectral acquisition was $\sim 1 \times 10^{-10}$ Torr. The C(1s) and N(1s) XP spectra were unchanged after collection of the NEXAFS data. Thus, effects due to beam-induced decomposition, fragmentation, or desorption appear to have been insignificant.

STM experiments were carried out using an Omicron UHV STM-1 instrument (base pressure 5×10^{-11} mbar). Images were acquired in constant current mode ($I_T = 1.0$ nA) with a negative tip bias ($U_{gap} = -1.0$ V). Image processing was limited to low-pass filtering unless otherwise described. Control experiments indicated that there were no tip-induced artifacts such as molecular displacement or adsorbate decomposition. Coadsorption experiments were carried out in a standing background pressure of 2×10^{-5} mbar H_2. TPR spectra (10 K s^{-1}) were obtained in a UHV chamber equipped with a quadrupole mass spectrometer. The latter was fitted with a collimator, and the crystal could be positioned at a distance of ~10 mm from the collimator aperture. Detection was therefore limited to species desorbing from the center of the front face of the crystal. Desorption data were corrected for instrumental sensitivity. Both the STM and the TPR apparatus incorporated LEED/Auger facilities used for surface characterization both prior to and during adsorption experiments. (*S*)-NEA (Fluka, Chiraselect >99.5%) was subjected to several freeze−pump−thaw cycles before use; the vapor, drawn from a warmed reservoir of the liquid, was introduced into the chamber where its purity was monitored by mass spectrometry.

3. Results and Discussion

3.1. X-ray Photoelectron Spectroscopy. C(1s) and N(1s) XP spectra were taken after (*S*)-NEA adsorption on Pt{111} at 300 K (data not shown). The C(1s) XP spectra consisted of two components with an integrated intensity ratio of ~5:1 and binding energies (BEs) of 284.7 ± 0.5 and 286.5 ± 0.7 eV, respectively. The lower BE component corresponds to the 10 carbon atoms in the naphthalene ring system (C_1-C_{10}), whereas the high BE component corresponds to the two carbon atoms in the ethylamine moiety (C_{11}, C_{12}, see Scheme 1). These assignments are in good accord with the XP spectra of closely related molecules,[23,24] and the observed 5:1 intensity ratio is consistent with the view that the molecular integrity of (*S*)-NEA is preserved upon adsorption on clean Pt{111}. The corresponding N(1s) XP spectrum contains only one peak centered at 399.7 ± 0.5 eV. After correction for the carbon and nitrogen atomic subshell cross sections at the relevant photon energy, the total carbon to total nitrogen ratio, C(total):N(total), determined from the normalized, integrated intensities, is 11.2 ± 1.0, in agreement with the expected stoichiometric value for molecular (*S*)-NEA (12:1). The surface coverage estimated from

(17) Bonello, J. M.; Lindsay, R.; Santra, A. K.; Lambert, R. M. *J. Phys. Chem. B* **2002**, *106*, 2672.
(18) Bonello, J. M.; Lambert, R. M. *Surf. Sci.* **2002**, *498*, 212.
(19) Stephenson, M. J.; Lambert, R. M. *J. Phys. Chem. B* **2001**, *105*, 12832.
(20) Stephenson, M. J.; Lambert, R. M., in preparation.
(21) Wehrli, J. T.; Baiker, A.; Monti, D. M.; Blaser, H. U. *J. Mol. Catal.* **1990**, *61*, 207.
(22) Briggs, C.; Seah, M. P. *Practical Surface Analysis*, 2nd ed.; Wiley-Interscience: Chichester, 1990; Vols. 1 and 2.
(23) Hitchcock, A. P.; Brion, C. E. *J. Electron Spectrosc. Relat. Phenom.* **1977**, *10*, 317.
(24) Robin, M. B.; Ishii, I.; McLaren, R.; Hitchcock, A. P. *J. Electron Spectrosc. Relat. Phenom.* **1988**, *47*, 53.

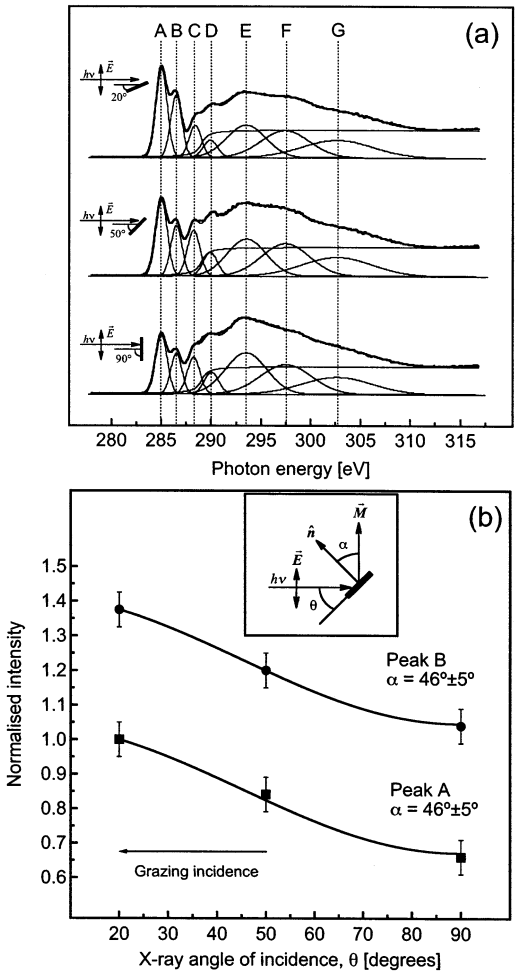

Figure 1. (a) Carbon K-edge NEXAFS spectra for (*S*)-NEA on Pt{111} at 300 K for 20°, 50°, and 90° incident photons. (b) Normalized π^* intensities for peaks A and B as a function of photon incidence angle.

the XP integrated intensities is $\sim 8.25 \times 10^{13}$ ($\pm 10\%$) (*S*)-NEA molecules cm^{-2}. This corresponds to 1 (*S*)-NEA molecule per 18 surface Pt atoms and is consistent with near-saturation coverages measured for similarly sized molecules on Pt{111} at 300 K.[5,25]

3.2. Near-Edge X-ray Absorption Fine Structure Spectroscopy. NEXAFS data were acquired at the carbon K-edge for a near-saturation coverage of (*S*)-NEA on Pt{111} at 300 K. The resulting spectra, shown in Figure 1a, exhibit seven discernible resonances at 285.0 (A), 286.4 (B), 288.3 (C), 290.0 (D), 293.5 (E), 297.5 (F), and 302.7 eV (G). Satisfactory fits were obtained when a single edge-jump was located at 289.1 eV.

The detailed spectral assignments are beyond the scope of the present publication and are given elsewhere.[26] The data were normalized following standard procedures,[27] and the molecular orientation determined from the variation in the π^* intensity associated with peaks A and B as a function of the photon incidence angle, θ, is 46° ± 5° with respect to the metal surface

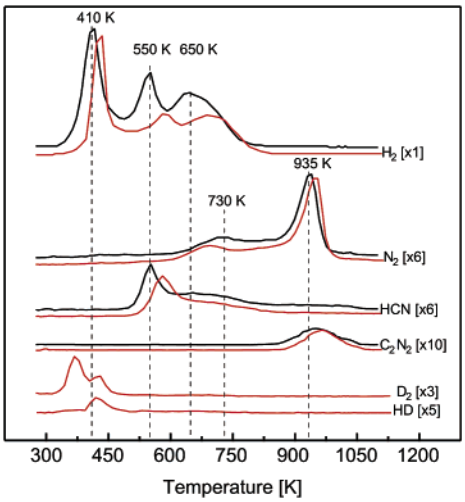

Figure 2. TPR spectra for (*S*)-NEA adsorbed on Pt{111} at 300 K.

(Figure 1b). Thus, on Pt{111} at near-saturation coverage, (*S*)-NEA molecules are strongly tilted at 300 K.

As we have discussed elsewhere,[18] because of the sensitivity of the tilt angle calculation to the π^* intensity measured at normal incidence, the value of 46° ± 5° represents an upper limit. In addition to the possible effect of lateral interactions in the adlayer, this tilt reflects molecule/surface interactions arising from the aromatic π-system and from the nitrogen lone pair. It seems likely that steric hindrance due to the ethylamine substituent at the 1 position also plays a significant role. That this is indeed so is strongly suggested by the tilt angles measured for quinoline and lepidine on Pt{111},[18] where we found α = 20° ± 5° and 32° ± 5°, respectively, with H and CH_3 at the 1 position on the aromatic system. Therefore, the secondary amine modifier derived from (*S*)-NEA is likely to be at least as strongly tilted as NEA itself. Interestingly, the observed π-resonance widths are in accord with these various adsorption geometries and the implied strength of the π-electron/surface interaction. Thus, in the case of quinoline,[18] stronger coupling of the "flatter" molecule to the metal results in a shorter excited-state lifetime and hence broader resonances. In the present case, where the molecule is more strongly tilted, we are able to resolve resonances A and B. Finally, as we shall show below, TPR data rule out the possibility that the large tilt angle found here is the result of H atom abstraction followed by binding of an NEA residue to the surface either via the ethylamine moiety or by σ bond formation with the aromatic ring carbons.

3.3. Temperature Programmed Reaction. The thermal behavior of (*S*)-NEA adsorbed on Pt{111} at 300 K provides useful auxiliary information. Saturation coverage TPR spectra (black lines, Figure 2) indicate that the principal desorption products were H_2 and N_2, along with smaller amounts of HCN and C_2N_2. The desorption of H_2 can be used to estimate the saturation coverage, yielding a value of $\sim 8.2 \times 10^{13}$ molecules cm^{-2} in agreement with the value calculated from the XPS data. The overall N:H ratio (calculated from the N_2 and H_2 integrated yields, corrected for instrumental sensitivity) is 1:12.3 ± 1, in accord with the value expected from the stoichiometry of the molecule (1:13). The hydrogen data exhibit peaks at 410, 550, and 650 K. Given that on Pt{111} H_2 desorption due to H_a recombination yields a peak at 330−370 K,[28] we may conclude that NEA adsorption at 300 K does *not* result in any C−H or

(25) Evans, T.; Woodhead, A. P.; Gutiérrez-Sosa, A.; Thornton, G.; Hall, T. J.; Davis, A. A.; Young, N. A.; Wells, P. B.; Oldman, R. J.; Plashkevych, O.; Vahtras, O.; Ågren, H.; Carravetta, V. *Surf. Sci.* **1999**, *436*, L691.
(26) Bonello, J. M.; Sykes, E. C. H.; Lindsay, R.; Williams, F. J.; Santra, A. K.; Lambert, R. M. *Surf. Sci.* **2001**, *482*−*485*, 207.
(27) Stöhr, J. *NEXAFS Spectroscopy*, 1st ed.; Springer Series in Surface Sciences Vol. 25; Springer: Berlin, 1996.

N−H bond cleavage. The observed peaks may therefore be attributed to a reaction rate-limited multistep decomposition of the adsorbate.[29]

On Pt{111}, aliphatic and aromatic C−H bond cleavage typically occurs at >350 K and >500 K, respectively.[29,30] NEA contains six H atoms in the ethylamine moiety and seven in the naphthalene ring. The ratio of integrated yields associated with the peak at 410 K to those at 500 + 650 K is 1:1.24 ± 0.2, in agreement with that expected from the stoichiometry of (*S*)-NEA (1:1.17). Furthermore, the H_2 peak at 410 K corresponds to hydrogen evolution associated with aliphatic C−H[29] and N−H[31,32] bond cleavage on Pt{111}. This confirms assignment of the 410 K peak to decomposition of the ethylamine moiety. As we shall see, the corresponding STM results indicate that destruction of this functional group begins at ∼325 K and is complete by ∼420 K. The hydrogen desorption features at 550 and 650 K very closely resemble the two-peaked spectrum observed for naphthalene decomposition on Pt{111}.[33] By analogy, we assign the 550 K process to the onset of dissociation of polymer chains (see STM results below), and the broader 650 K process is assigned to dehydrogenation of the resulting C_xH_y hydrocarbon fragments.[33] For present purposes, the nitrogen TPR spectrum is not of primary interest. The 730 K process is most likely the result of the N(a) recombination following H_xCN(a) and CN(a) decomposition.[31,32] The feature at 935 K is probably associated with a surface nitride species: it occurs widely in TPR of N-containing compounds on Pt{111}.[31]

A typical TPR spectrum following coadsorption of (*S*)-NEA and deuterium is also shown in Figure 2 (red lines). The surface was predosed with deuterium, prior to exposure to (*S*)-NEA. The only deuterated desorption products observed were D_2 (370 and 430 K) and HD (430 K). In regard to the other species, the TPR data obtained in the absence and presence of coadsorbed deuterium are remarkably similar in regard to both peak positions and relative intensities. Therefore, as in the absence of coadsorbed D_a, the results suggest that dissociation of the aliphatic ethylamine moiety occurs before the decomposition of the aromatic naphthalene group. This is corroborated by the STM images taken for (*S*)-NEA in the presence of a standing background of hydrogen (see below), which suggest that dissociation of the ethylamine moiety occurs in the presence of hydrogen. Note that, in the presence of coadsorbed deuterium, the onset of hydrogen evolution ascribed to the dissociation of the ethylamine moiety occurs at a slightly higher temperature than that in the absence of coadsorbed deuterium. This is consistent with the need to desorb D_a, thus liberating surface sites required for dissociation of the ethylamine moiety.

3.4. Scanning Tunneling Microscopy. Variable temperature STM images were acquired both as a function of temperature and in the presence and absence of a standing background pressure of hydrogen. The temperature range chosen for these measurements encompasses that in which collapse of enantioselectivity occurs during the catalytic reaction.[5−8]

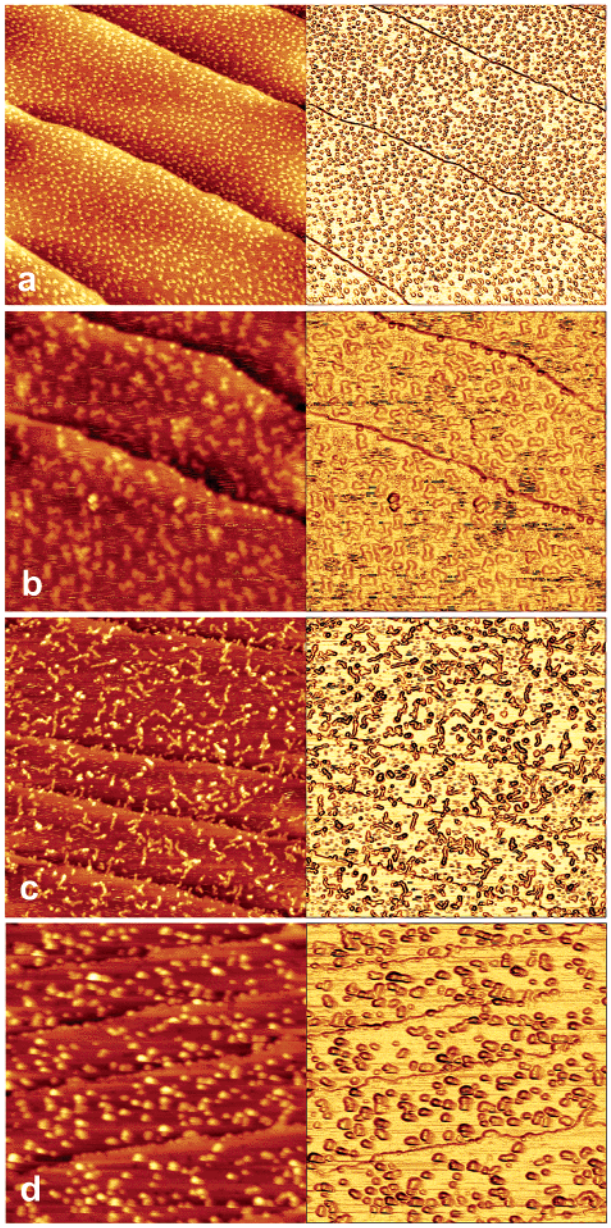

Figure 3. STM images (raw data and edge contrast enhanced) of (*S*)-NEA on Pt{111} in the absence of coadsorbed hydrogen at (a) 298 K (500 Å × 500 Å), (b) 370 K (250 Å × 250 Å), (c) 495 K (600 Å × 600 Å), and (d) 650 K (600 Å × 600 Å).

Hydrogen Absent. STM images for (*S*)-NEA adsorbed on Pt{111} in the absence of coadsorbed hydrogen are shown in Figure 3a−d. The initial surface coverage measured directly from Figure 3a is $\sim 8 \times 10^{13}$ molecules cm^{-2}. In Figure 3a, elongated features corresponding to individual (*S*)-NEA molecules are readily discerned. The average dimensions of these features are (8.30 ± 0.8 Å) × (8.46 ± 0.8 Å) × (2.02 ± 0.2 Å) (length × breadth × height), consistent with the analogous van der Waals dimensions for naphthalene (8.12 Å × 7.36 Å × 3.4 Å[34,35]). The apparent STM height for naphthalene[35,36] and quinoline[18] on Pt{111} is ∼1 Å. For (*S*)-NEA, the corresponding value is ∼2 Å. These heights are in excellent qualitative accord

(28) Christmann, K.; Ertl, G.; Pignet, T. *Surf. Sci.* **1976**, *54*, 365; *Surf. Sci.* **1976**, *60*, 365.
(29) Wilk, D. E.; Stanners, C. D.; Shen, Y. R.; Somorjai, G. A. *Surf. Sci.* **1993**, *280*, 298.
(30) Friend, C. M.; Muetterties, E. L. *J. Am. Chem. Soc.* **1981**, *103*, 773.
(31) Gland, J. L. *Surf. Sci.* **1978**, *71*, 327; *Surf. Sci.* **1981**, *104*, 478.
(32) Hwang, S. Y.; Seebauer, E. G.; Schmidt, L. D. *Surf. Sci.* **1987**, *188*, 219.
(33) Dahlgren, D.; Hemminger, J. C. *Surf. Sci.* **1982**, *114*, 459.
(34) Gland, J. L.; Somorjai, G. A. *Surf. Sci.* **1973**, *38*, 157.
(35) Chiang, S. *Chem. Rev.* **1997**, *97*, 1083.
(36) Hallmark, V. M.; Chiang, S.; Brown, J. K.; Wöll, Ch. *Phys. Rev. Lett.* **1991**, *66*, 48.

with our NEXAFS results, which, it may be recalled, yield tilt angles of 20° ± 5° (quinoline) versus 46° ± 5° (NEA). Although not visible as a distinct entity, the presence of the ethylamine moiety is in accord with the imaged lateral dimensions of (*S*)-NEA, these being somewhat larger than those recorded for naphthalene itself.[35,36]

Most significantly, no long-range order is apparent, in accord with LEED observations which showed no new adsorbate-induced features. This is in opposition to the so-called template model of chiral induction, according to which the formation of suitably spaced arrays of adsorbed chiral (*R* or *S*) entities generates intrinsically chiral (*R* or *S*) vacant adsorption sites, which orient the incoming pyruvate reactant so as to provide the required enantiospecificity in the subsequent hydrogenation step. On the other hand, our results are at least consistent with the 1:1 interaction model of chiral induction,[5−8] which calls for a 1:1 docking interaction between randomly distributed chiral modifier molecules and the incoming pyruvate.

Heating to ∼325 K (data not shown) led to the onset of a process whose completion is illustrated in Figure 3b, where the image was acquired at 370 K. This process includes two important and distinct effects. First, it is clear that molecular agglomeration occurred, resulting in formation of characteristic "dog-bone" dimers, implying chemical reaction between (*S*)-NEA molecules. Recall that the TPR data indicate that decomposition of the ethylamine moiety by hydrogen elimination begins around this temperature, thus destroying the amine center believed to be involved in the crucial interaction with the α-ketoester reactant in the enantiodifferentiation step. Second, this agglomeration acts to denude the surface of chirally modified adsorption sites, hence increasing the number of unmodified or racemic Pt sites. In concert, these effects could act to cause the collapse of enantioselective behavior. Their onset at ∼325 K coincides with the commonly reported temperature for the observed loss of enantioselectivity,[5−8] providing the first direct clue as to the possible origin of enantioselectivity collapse in the Orito reaction. Reducing the temperature showed that these effects were irreversible.

The dog-bone dimers were not very mobile on the surface at ∼325 K and were stable over several days. Their average dimensions are in agreement with the van der Waals dimensions for two adjacent naphthalene molecules, indicating that the aromatic ring remains intact during dimerization. However, they exhibited greater corrugation relative to the (*S*)-NEA monomers (2.69 ± 0.3 Å versus 2.02 ± 0.2 Å, respectively). Although dimer formation was the principal mode of self-reaction, some higher order structures were also occasionally observed. These corresponded to the interaction of three and even four (*S*)-NEA molecules, yielding propeller and rhomboid structures. With increasing temperature, further self-reaction resulted in progressive linear and dendritic chain growth, and Figure 3c illustrates the STM image taken at 495 K by which stage the process was complete. It is apparent that chains were fairly evenly distributed across the terraces, although with some tendency for step edge decoration. The most common linear chain length was 40 ± 5 Å (∼5 naphthalene units), and the longest straight chain measured was 84 ± 8 Å (∼10 naphthalene units). The largest dendritic structure had a total length of 210 ± 10 Å (∼25 naphthalene units). The polymerization process presumably involves Diels−Alder-type cycloaddition of the naphthyl units

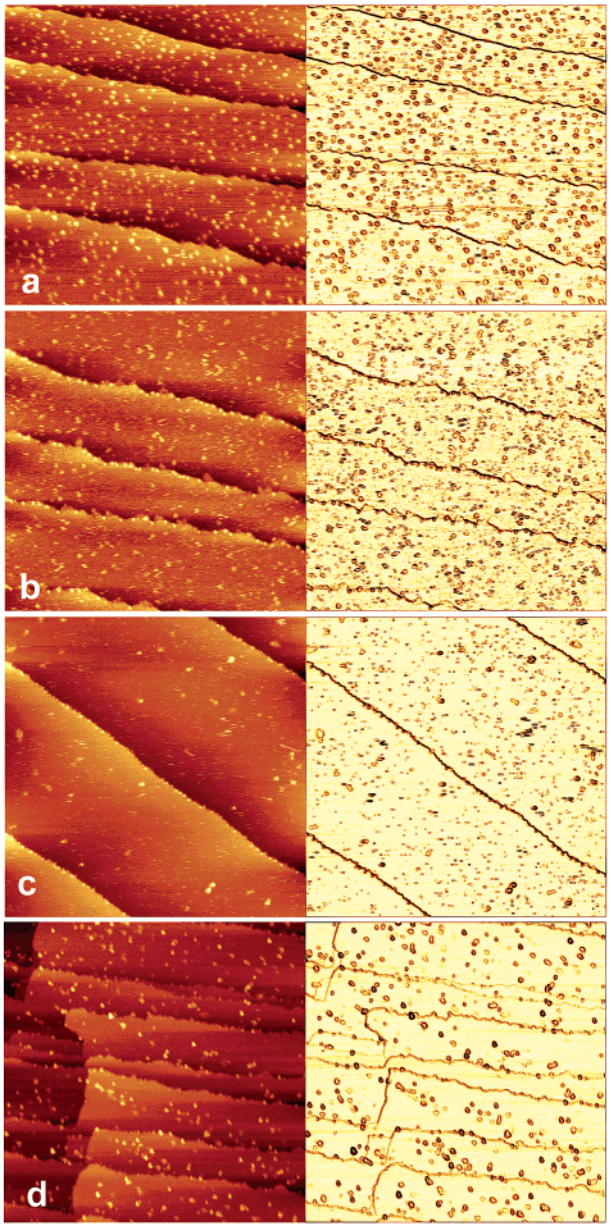

Figure 4. STM images (raw data and edge contrast enhanced) of (*S*)-NEA on Pt{111} in the presence of coadsorbed hydrogen at (a) 298 K (500 Å × 500 Å), (b) 370 K (500 Å × 500 Å), (c) 460 K (500 Å × 500 Å), and (d) 650 K (1000 Å × 1000 Å).

remaining after decomposition of the dog-bone dimers. At ∼520 K, the polymeric structures began to dissociate, with accumulation of the resulting debris both at step edges and on the terraces. The polymers were in an advanced state of decomposition by ∼560 K, and by 650 K (Figure 3d) the C KLL Auger intensity indicated that the residues formed retained all of the original carbon; a weak N KLL signal was also observed but not quantified. The TPR data suggest that beyond 650 K this residue decomposes, producing C(a), H_2, N_2, HCN, and C_2N_2.

With Coadsorbed Hydrogen Present. The behavior of (*S*)-NEA in the presence of coadsorbed hydrogen was studied by first dosing the clean surface with hydrogen, then with (*S*)-NEA, and finally imaging in a standing pressure of 2×10^{-5} mbar H_2. The resulting images are shown in Figure 4a−d and correspond to an initial coverage of $\sim 7.8 \times 10^{13}$ molecules cm^{-2}. As in the absence of coadsorbed hydrogen, at 298 K,

(*S*)-NEA molecules were randomly but uniformly distributed on the Pt{111} terraces (Figure 4a). The measured average molecular dimensions ((8.28 ± 0.8 Å) × (8.54 ± 0.8 Å) × (2.08 ± 0.2 Å)) and corrugation (2.08 ± 0.2 Å) are well in accord with those obtained in the absence of hydrogen. Thus, coadsorbed hydrogen appears not to alter substantially either the adsorption geometry or the spatial distribution of NEA. The center-to-center separation between molecules is 8−12 Å, there is some tendency for accumulation at step edges, the molecules do not align themselves along any particular crystallographic axis, and there is no discernible long-range order. This provides even stronger evidence against the template model and, again, is at least consistent with the 1:1 interaction model of chiral induction.

Dramatic changes occurred at ~370 K (Figure 4b). First, the terraces were denuded of molecules accompanied by pronounced accumulation of material at step edges. Second, although there was some evidence of dimer formation, most features exhibited an apparent height similar to that of naphthalene (~1 Å), rather than (*S*)-NEA (~2 Å). In accord with this, these species had lateral dimensions characteristic of naphthalene *without* the ethylamine moiety. Recall that the TPR data for desorption of (*S*)-NEA in the presence of D_a indicate that dissociation of the ethylamine moiety occurs at this temperature. These changes were irreversible and occurred in the temperature range corresponding to enantioselectivity collapse in chiral hydrogenation.[5−8] It appears that the reactivity of the ethylamine function in (*S*)-NEA is entirely different in the absence and presence of coadsorbed hydrogen: dimerization with hydrogen elimination versus dissociation of the ethylamine moiety. Both processes, however, result in destruction of the critically important amine center.

By ~400 K (not shown), the majority of naphthalene molecules residues had diffused to the step edges, the presence of streaks suggesting pronounced adsorbate mobility. A few features remained on the terraces whose lateral dimensions corresponded to either individual naphthalene molecules or dog-bone dimers. No significant changes occur at ~460 K (Figure 4c), although clusters of debris resulting from naphthalene decomposition[36] appear both on the terraces and at step edges. By ~650 K (Figure 4d), only randomly distributed clusters of debris remained, the Auger spectrum implying no loss of carbon.

With Coadsorbed Methyl Pyruvate in the Absence and Presence of Hydrogen. Finally, we investigated the behavior of (*S*)-NEA in the presence of coadsorbed methyl pyruvate (the prochiral reactant) in the absence and presence of coadsorbed hydrogen. The latter is as close to actual reaction conditions as we can get. In the first case, (*S*)-NEA was preadsorbed, followed by methyl pyruvate (MP). In the second case, hydrogen was preadsorbed, then (*S*)-NEA, and finally MP, imaging being carried out in a standing pressure of 2×10^{-5} mbar H_2.

We have already studied the adsorption properties of methyl pyruvate on Pt{111} in the absence and presence of hydrogen.[37] In the absence of H_a, methyl pyruvate undergoes extensive polymerization at 298 K; however, the presence of H_a suppresses this reaction. Figure 5a shows an STM image obtained after codosing (*S*)-NEA and MP at 298 K in the absence of H_a. It appears that MP undergoes some self-reaction, although comparison with our earlier data[37] reveals that this is much less extensive in the presence of (*S*)-NEA.

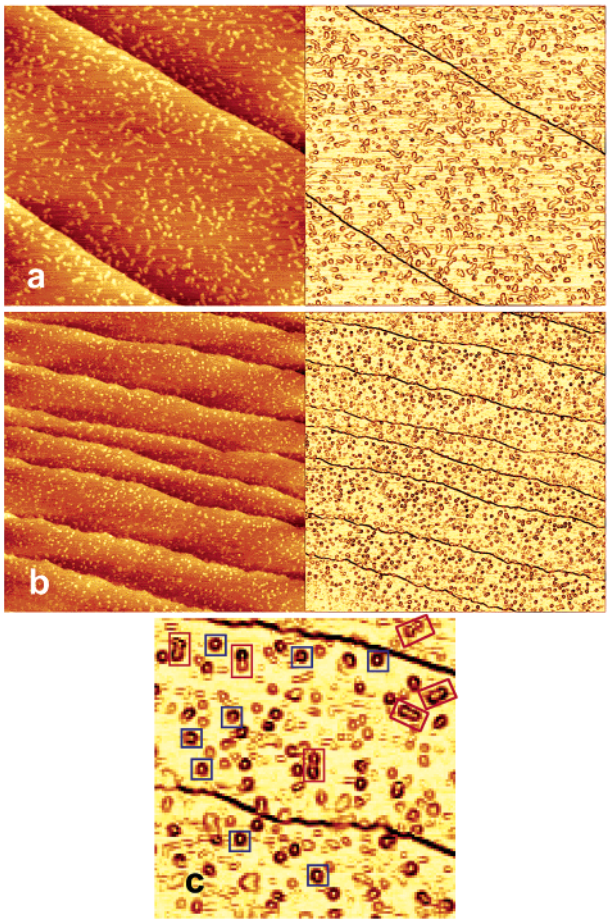

Figure 5. STM images (raw data and edge contrast enhanced) of (*S*)-NEA on Pt{111} in the presence of coadsorbed methyl pyruvate at 298 K (a) in the absence of H_a (1000 Å × 1000 Å), (b) with coadsorbed hydrogen (1000 Å × 1000 Å), and (c) as (b) but magnified to show what happens (250 Å × 250 Å).

The picture is very different in the presence of H_a − which completely suppresses the self-reaction of MP.[37] Figure 5b shows the result. Again, there is no long-range order, another negation of the chiral template hypothesis. The most intriguing features are visible in Figure 5c, which shows a magnified portion of 5b. Here we see single entities (blue boxes), which, according to their dimensions, are individual molecules (MP and (*S*)-NEA have similar dimensions as measured by STM). However, we also see some larger entities (red boxes). Clearly, they are *not* NEA dog-bone dimers, and their length is twice the average of NEA and MP. They are also unsymmetrical. It is tempting, although admittedly speculative, to assign these objects a 1:1 *docking complex* between the prochiral reactant (MP) and the chiral modifier ((*S*)-NEA).

4. Conclusions

(1) At 300 K, (*S*)-NEA molecules do not form ordered arrays on Pt{111}. Coadsorption with hydrogen, methyl pyruvate, or methyl pyruvate + hydrogen also does not induce the formation of ordered structures. These results provide the first direct evidence against the template model and are at least consistent with the 1:1 interaction model of chiral induction in the enantioselective hydrogenation of alkyl pyruvates.

(37) Bonello, J. M.; Williams, F. J.; Santra, A. K.; Lambert, R. M. *J. Phys. Chem. B* **2000**, *104*, 9696.

(2) In the absence of hydrogen, above 320 K − the temperature of enantioselectivity collapse − dimerization with hydrogen elimination occurs. This destroys the amine center involved in the enantiodifferentiation step and also acts to denude the surface of chirally modified adsorption sites. In concert, these processes should result in enhanced racemic hydrogenation at the expense of the enantioselective reaction.

(3) Raising the temperature beyond 320 K in the presence of coadsorbed hydrogen (or deuterium) results in destruction of the ethylamine moiety.

(4) The effects described under points 2 and 3 are irreversible. They provide the first direct clue as to the possible origin of enantioselectivity collapse in hydrogenation of α-ketoesters on platinum surfaces, by a mechanism not previously considered.

(5) The π-system of (*S*)-NEA is strongly tilted on Pt{111} at 300 K ($\alpha = 46° \pm 5°$). The secondary amine formed under reaction conditions is likely to be even more strongly tilted. Comparison with related data suggests that the often-made assumption of a flat-lying aromatic moiety under reaction conditions may need closer examination.

(6) When NEA and methyl pyruvate are coadsorbed in the presence of H_a, STM reveals entities that could correspond to a 1:1 docking complex between the prochiral reactant and the chiral modifier.

Acknowledgment. This work was supported under Grant GR/M76706 provided by the U.K. Engineering and Physical Sciences Research Council. J.M.B. acknowledges the award of a CVCP Overseas Scholarship and additional support from the Cambridge University Oppenheimer Fund and King's College, Cambridge. F.J.W. acknowledges the award of a Cambridge University Oppenheimer Research Fellowship.

JA028436X